



The study on the synthetic methodologies for manoeuvring the morphology crystallinity and particle size of hydroxyapatite

J. Anita Lett^{1*}, K. Ravichandran² and M. Sundareswari¹

¹Department of Physics, Sathyabama University, Chennai, India

²Department of Analytical Chemistry, University of Madras, Chennai, India

ABSTRACT

The synthetic Hydroxyapatite (HAp) nanoparticles are extensively used to significantly improve the biocompatibility and bioactivity of man-made biomaterials. A wide variety of methods are available for the preparation of HAp nanoparticles, choosing a procedure to synthesize it for specific requirement is laborious. Hence, in our present investigation we try to evaluate the Hydroxyapatite crystals synthesized in four different methodologies. The methodologies used to synthesis the hydroxyapatite nanoparticles via hydrothermal, sol-gel, precipitation and microwave methods. The calcium and phosphorus precursors were chosen with molar ratio of 1: 0.6 to achieve the synthetic bone like apatite. The prepared samples with different synthetic methods were characterized using XRD, FE-SEM, EDAX and Raman to ascertain the crystalline size, phase structure, morphology, stoichiometric ratio and the functional groups present in the resultant hydroxyapatite nanoparticles.

Key words: Biomaterials, Hydroxyapatite, Nanoparticles, Hydrothermal, Microwave.

INTRODUCTION

Hydroxyapatite (HAp) is the principal inorganic constituent present in hard tissues, dental enamels and dentins of Homosapiens, possessing a molecular formula of $\text{Ca}_{10}(\text{PO}_4)_6(\text{OH})_2$. Hydroxyapatite ceramics belongs to a class of phosphate-based materials, which have been widely used as bone substitutes. Due to the chemical similarity between HAp and mineralized bone of human tissue, synthetic HAp exhibits strong attraction to bone hard tissue. Formation of chemical bond with the host tissue offers HAp a greater advantage in clinical applications than most other bone substitutes. Synthesising of HAp with similar properties to that of natural one is the most explored topic of extensive biological and physico-chemical research [1-2]. The HAp exhibits properties like biocompatibility, biological activity, osteo-inductivity, osteo-conductivity, osseo-integration, stable bioresorption, strong ion exchange capacity and ability to promote bone ingrowths besides aiding regeneration of new bones [1-4]. Hence, it is used widely as dental filler material, bone & bone graft substitutes in orthopaedic applications, hard tissue paste, tissue engineering [5-6], biological sensors [7-9], drug carriers/ delivery devices [10-11] and alveolar ridge [12].

However, synthetic HAp find only limited use in load bearing applications due to low toughness (0.8-1.2 MPa. \sqrt{m}), poor flexural strength (<140 MPa), high brittleness and lower hardness [5, 13-14]. These limitations are overcome either by physical incorporation of suitable materials viz. polymers [15-16], metals nano particles [17-20], metal oxides [21-23], carbon materials [4, 24] etc., or by adopting suitable processing techniques such as thermal spraying, microwave processing and sintering to enhance the mechanical properties required for load bearing applications. On the other hand, the reduction of particle size from micro to nano level also significantly improves the mechanical properties, toughness and hardness of the HAp besides improving their biological activities [3, 5, 14]. Moreover the addition and/or replacement (substitution or co-substitution) of metal ions viz., Na, K, Ag, Zn, Mg, Sr, Cu, Ba, Fe, Ce, Si, Bi, Ti and Cd instead of calcium in the HAp lattice also improve the mechanical properties along with solubility, crystallinity, morphology, lattice parameters and biological activity [3, 25-33].

Synthetic wet methods, yielding tailor made particle size and morphology to improve the mechanical properties are found to be highly attractive. Various synthetic routes are reported under the wet chemical preparation of HAp. The most important methods being chemical precipitation, hydrolysis, sol-gel, hydrothermal, micro emulsion, molecule direct crystallization, bio-mineralization, diffusion, gravity-assisted, microwave assisted, precursor transformation and sonochemical methods [1-2]. Hence, it is pertinent to identify an inexpensive and simple methodology, which facilitates the precise control of particle size, morphology and chemical composition. Further these methods depend on the controlled parameters such as nature and concentration of precursors, additives, reaction temperatures, pH, aging temperature, duration of aging, calcination temperature and duration of calcinations to produce required particle size and morphology [2, 34-36].

The chemical precipitation, hydrothermal, sol-gel and microwave methods facilitate the precise control of the above parameters. These methods are versatile in energy efficiency, economic, eco-friendly, manageable time and ease of operation without warranting high end equipment. Though there are certain limitations associated with each of these methods, the present work aims at comparing the suitability of these methods in preparing a pure phase, crystalline HAp with required morphologies and particle sizes under our experimental conditions.

EXPERIMENTAL SECTION

2.1. Materials

Reagent grade calcium nitrate tetra hydrate ($\text{Ca}(\text{NO}_3)_2 \cdot 4\text{H}_2\text{O}$), diammonium hydrogen phosphate ($(\text{NH}_4)_2\text{HPO}_4$) and liquid ammonia (NH_3) from Merck chemical were used.

2.2. Architecture of HAp

The precursors used in the study of Precipitation (PP), hydrothermal (HT), sol-gel (SG) and microwave (MW) preparation of hydroxyapatite were calcium nitrate tetrahydrate ($\text{Ca}(\text{NO}_3)_2 \cdot 4\text{H}_2\text{O}$) as a source of calcium ions and diammonium hydrogen phosphate ($(\text{NH}_4)_2\text{HPO}_4$) as the phosphorus precursors. The molar ratio of precursors Ca/P was taken as 1.67. The precursors were maintained same for all the preparation methods. A solution of 0.6M $(\text{NH}_4)_2\text{HPO}_4$ was added drop wise into 1M $\text{Ca}(\text{NO}_3)_2 \cdot 4\text{H}_2\text{O}$ solution with continuous stirring at room temperature for two hours resulting in white precipitate. Using ammonia solution the final pH was adjusted to 11.0. The chemical equation that describes the formation of HAp is



In precipitation and microwave synthesis, after the above step the aging was done under continuous stirring in room temperature for 24 hours. The white precipitate obtained was filtered and washed repeatedly with distilled water in precipitation method, whereas in microwave synthesis after aging, the resultant suspension was exposed to microwave irradiation for 25 minutes in a domestic microwave oven. The hydrothermal synthesis involves aging of the reaction mixture in an autoclave for 2 hours at 150°C. Then, suspension was allowed to cool naturally followed by filtering. In the sol-gel process, $\text{Ca}(\text{NO}_3)_2 \cdot 4\text{H}_2\text{O}$ sol was prepared using ethanol and stirred for 1 hour. This sol was added drop wise into the $(\text{NH}_4)_2\text{HPO}_4$ solution with vigorous stirring at a temperature of 85°C. The pH was adjusted at 11.0 using liquid ammonia. The prepared solutions were transformed into a white gel after a period of 4 hours and it is further aged at room temperature for 24 hours. The aged gel was dried at 100°C for 24 hours. The HAp crystals obtained with these methods were ground with a mortar and pestle and sintered at 800°C in a muffle furnace under an air atmosphere for 2 hr. Thus obtained samples were subjected to further characterization.

2.3. Characterizations

2.3.1. Functional group Identification: Raman measurements were carried out using laser light 510nm excitation source using confocal Raman spectroscopy (Nanophoton Raman-11i). The Raman spectra of the samples were obtained in the spectral range from 2500 to 0 cm^{-1} . All samples were analysed with similar transmission for the sake of comparison purpose of peak intensity with crystallinity.

2.3.2. Phase analysis: Phase analysis of thus organized HAp were carried out by the X-ray diffraction (XRD) technique using a diffractometer (X'pertPro, Philips, Netherlands). The 2Θ scanning range was from 10°-90° with step time of 1 sec and step size of $2\Theta=0.1^\circ$. Debye-Scherrer approximation was used to compute the average crystallite size.

$$D_{\text{hkl}} = K\lambda / \beta \cos\theta \quad (2)$$

where: K = constant dependent on crystallite shape, $0.8 < K < 1.1$; K = 0.94 for FWHM of spherical crystals with cubic symmetry; λ is the wavelength of monochromatic radiation ($\lambda = 1.5405\text{\AA}$). β is defined as the full width of

peak from the intensity distribution pattern measured at half of the maximum intensity value. D_{hkl} is the particle size, as calculated from (hkl) reflections, λ is the wavelength Cu $K\alpha$ radiation (1.54060Å), β refers to the full width at half maximum for the diffraction peak under consideration (in radians), Θ is the diffraction angle ($^\circ$).

The degree of crystallinity (X_c) can be evaluated by the following equation 3 based on the previous reports (37).

$$X_c = (0.24/\beta)^3 \quad (3)$$

Where β represents the full width at half maximum for the precise diffraction peak of miller's plane.

2.3.3. Microstructural characterizations: The microstructures and morphologies of the HAP crystals were studied by field emission scanning electron microscope (FESEM: Supra VP35 Carl Zeiss, Germany). The energy dispersive X-ray (EDX: X-Max, USA) spectra were obtained by a standard unit (Oxford Instruments, UK) attached to the FESEM.

RESULTS AND DISCUSSION

3.1. Raman Studies:

The Raman spectra of the samples are depicted for all the four methods in Fig. 1.0. The spectrum for HAp shows bands at 428, 583, 959, 1042 and 1071 cm^{-1} . The peak at 428 cm^{-1} corresponds to the factor group splitting of the ν_2 bending vibrations of the PO_4^{3-} ion, the peak at 583 cm^{-1} corresponds to ν_4 fundamental vibrational mode which arises from the triply degenerate bending vibrations. The band at 959 cm^{-1} corresponds to the symmetric stretching modes and is designated as ν_1 fundamental vibrational mode. The two peaks at 1042 cm^{-1} and 1071 cm^{-1} are due to ν_1 asymmetric stretching vibrations of the P–O bonds [38-40]. The peak intensity in the Raman spectra is an indication of crystallinity [41]. From our experimental conditions the peak intensity is in the order of MW, PP, SG and HT methods. The MW method reveals higher crystallinity and may be due to the homogeneous heat distribution during the crystal formation and the possibility of higher orientation.

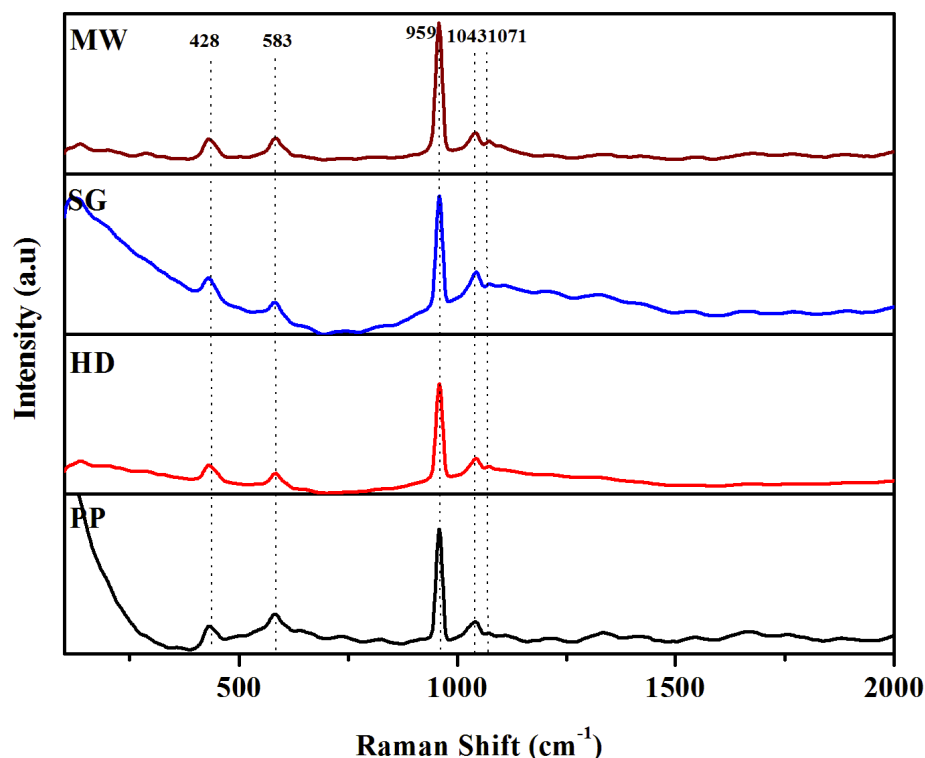


Figure.1 Raman spectra of HAp synthesized using four different method

3.2. FESEM studies :

FESEM morphology of the samples obtained by the different method is shown in Fig.2. In precipitation method highly agglomerated crystals with uneven structures were observed (figure.2.a.). Numerous spherical and plate like crystals were observed and are found agglomerated together to form a rod like shapes. Renu Sharma et al have reported the formation of micro-structured HAP with similar morphology with a strong dependence of morphological

features of HAp with respect to the final pH of the solution during synthesis [42]. The attributed agglomeration may be due to hydrogen bonding ability between HAp particles and also due to higher affinity of Hydroxyapatite particles to form different phase of calcium phosphates [43-46].

Hydrothermally synthesized HAP sample (Fig.2.b) showed a well distinct and uniformly distributed spherical plate like crystals with insignificant agglomeration. Previous reports counseled the formation of HAp retaining plate (47), sphere (48), whiskers (36, 49), cubic, feather (50) and rod (51) like morphological features on varying experimental parameters like chemical composition, pH, ageing temperature and time, and sintering temperature (52). Mehdi Sadat-Shojai *et al* reported that the HAp nanoparticles synthesized at alkaline conditions were more spherical or close to spherical in shape and around 50 nm in size, although some particles could also elongate up to maximum ~150 nm, resulting in very short nanorods. Architecture of spherical morphology is anticipated due to the high pH value, ensuring an isotropic or weak-anisotropic growth by adsorption of OH⁻ ions strongly on the calcium phosphate crystals resulting in spherical nanoparticles or at most very short nanorods. Simultaneously, at lower pH an anisotropic growth occurs, crystals cultivate them as either one-dimensional nanorods / two-dimensional nanoplates / three-dimensional feathery structure / three-dimensional micro cubes, or three-dimensional microfibers. Indeed, an entangled shape of the CaP crystals can be formed at lower pH [50, 53].

The Hydroxyapatite synthesized by sol-gel (SG) showcases smaller particles with irregular shape (spherical, needle and quasi spherical) agglomerated non-uniformly (Figure.2.c). Solution parameters, aging time and dropping time plays a major role in controlling particle dimensions. Spherical shape are harvesting by quick addition of phosphate precursor aqueous solution into (Ca(NO₃)₂) ethanol solution under vigorous stirring, where as slackened addition results in nanorods. [54]. Calcium nitrate when used as calcium precursor forms HAp particle that are spherical and agglomerated [55]. The aging time has an impact on particle size. The particle size decreases from micron to nano with increase in ageing time. Based on the above inferences, we can justify the result for the performed investigational situation with calcium nitrate as calcium precursor and aging conducted for 24 hour.

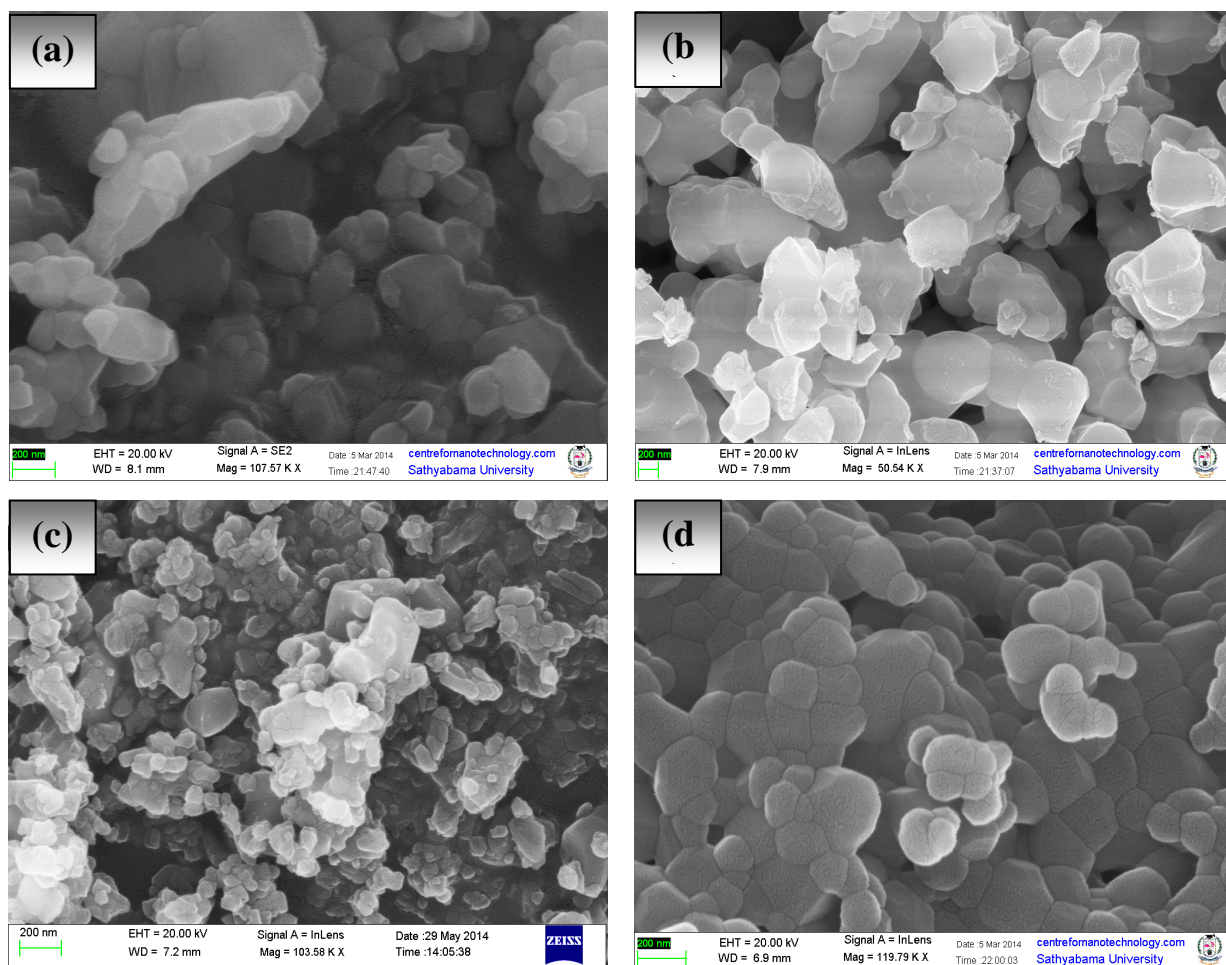


Figure.2 Field Emission Scanning Electron Micrographs of HAp synthesized using (a) PP, (b) HT, (c) SG and (d) MW

The samples produced by microwave method (Fig.2.b) were spherical and agglomerated with unique network like dimension. Siwaporn Meejoo *et al* prepared a nano HAP via precipitation followed by microwave irradiation with particle size around 100 nm as well as these results are in good agreement with our results. The particle agglomerations can be due to (i) the short range of force in which the particles are held together (ii) the force between the particles may be electrostatic or van der Waal's attractions (iii) liquid capillary forces due to presence of liquid within the granules [56]. Byong-Taek Lee *et al* studied the synthesis of HAP and biphasic tricalcium phosphate (BCP) powder with effect of pH and microwave heating and reported the formation of spherical particle due to the shorter reaction time in the microwave system which inhibits the further crystal growth. The higher energy supplied in short time during irradiation could be a reason for the decrease of the surface energy of the synthesized particles and thus hinders the further crystal growth [57].

3.3. EDX studies:

The EDX spectrum of HAP samples were shown in Fig. 3. The data confirmed the presence of calcium and phosphate. Based on the EDX analysis the ratio of Ca/P was calculated as 1.87, 1.68, 1.54 and 1.77 for PP, HT, SG and MW methods respectively. The precipitation method showed higher Ca/P ratio due to more complex reaction with different phases of calcium phosphate formation under our experimental condition. The hydrothermally synthesized HAP was highly stoichiometric due to the elevated aging temperature. The lowered Ca/P ratio in sol-gel method can be accounted due to slower reaction by the gelation process and formation minor quantities β -TCP, the presence of β -TCP is further supported by the XRD analysis. Due to the faster reaction rate and effective transformation of energy the microwave synthesis offered slightly higher stoichiometric HAP. Form the calculated results the stoichiometric ratio of Ca/P was found to vary from 1.54 to 1.87 in the order of SG>HT>MW>PP methods.

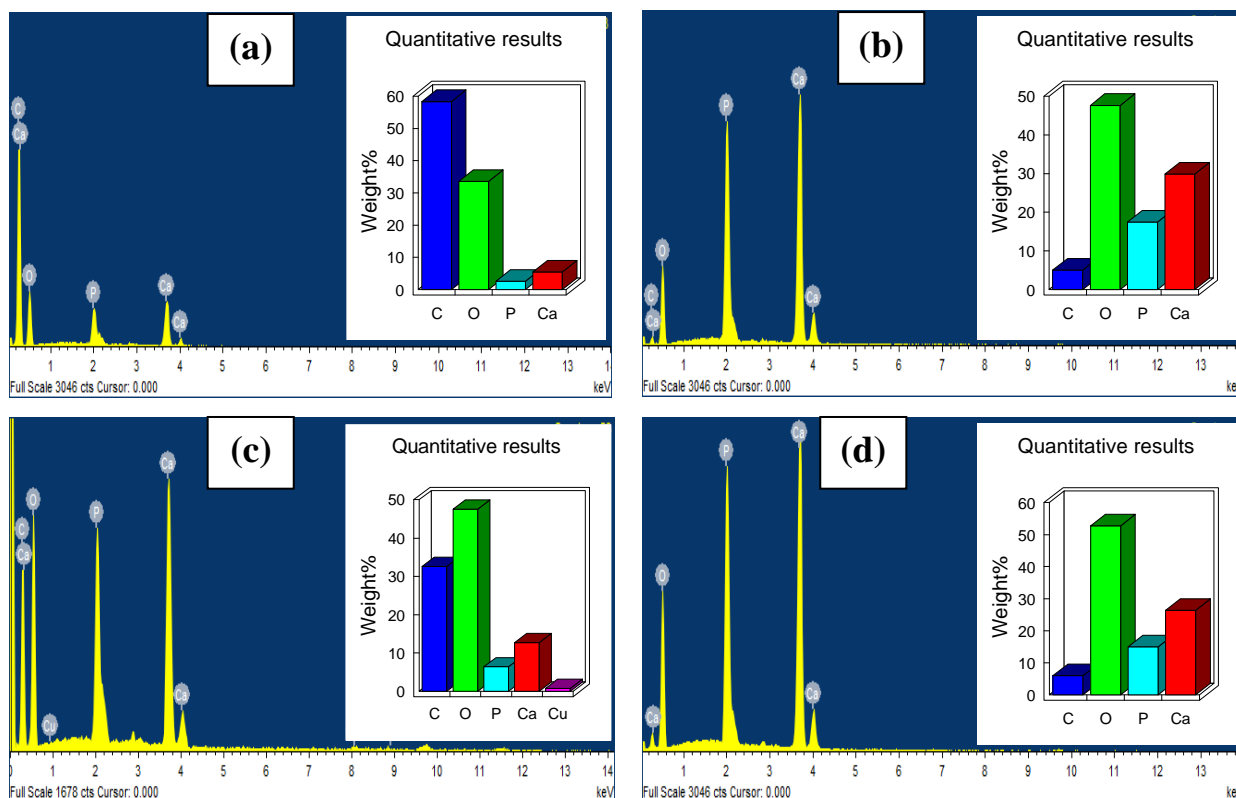


Figure.3 EDX spectrum and quantitative results of HAP synthesized using (a) PP (b) HT (c) SG and (d) MW

3.4. XRD Studies:

The XRD pattern of all the synthesized HAP is presented in the figure.4 and the crystal structure studies are shown in figure.6. The diffraction patterns show sharp and clear reflections however with varying intensity which confirm the phase purity and crystallinity associated with each of the samples. The XRD pattern, with major diffraction peaks located at $2\theta = 25.9^\circ$ (002), $2\theta = 31.7^\circ$ (211), $2\theta = 32.1^\circ$ (112), $2\theta = 32.8^\circ$ (300), $2\theta = 46.6^\circ$ (222) and $2\theta = 49.4^\circ$ (213) are found to match with ICDD - PDF2 card: 00-009-0432. These data confirm that the major phase as hydroxyapatite particles. Absence of calcium phosphates and calcium oxide are clearly identified except for sample prepared by sol-gel method. The crystallite sizes obtained were in the range of 43 to 106 nm. The particle size was varied in the order MW ($\approx 106\text{nm}$) > PP ($\approx 62\text{nm}$) > SG ($\approx 48\text{nm}$) > HT ($\approx 44\text{nm}$) (Fig.5.0). The crystallinity of the samples was

calculated based on equation 3.0. The degree of crystallinity is also found to be in the same order to that of particle size ie.17.23>4.02>1.85>1.39 respectively for MW, PP, SG and HT. Higher alkaline conditions are reported to produce phase pure HAp, phase purity observed with our samples are thus justified. As discussed earlier the crystal size and crystallinity of HAp are influenced by reaction conditions and path way.

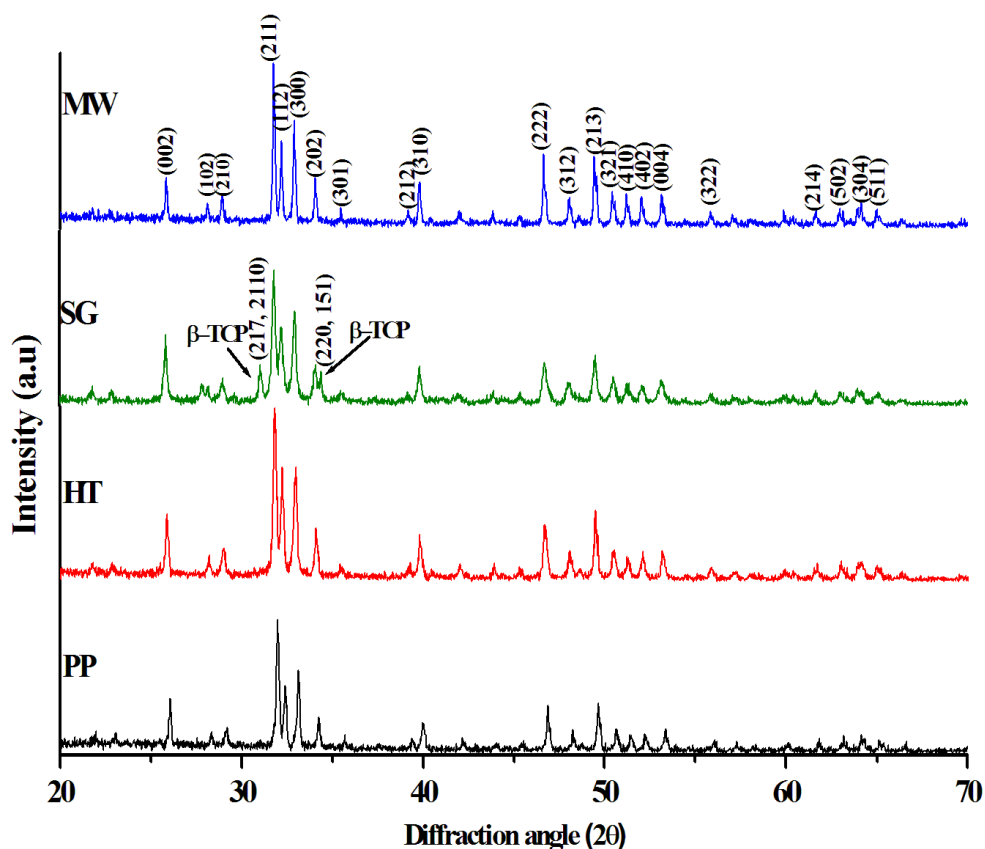


Figure.4 X-Ray Diffraction studied of HAp synthesized using four different Methods (PP, HT, SG and MW)

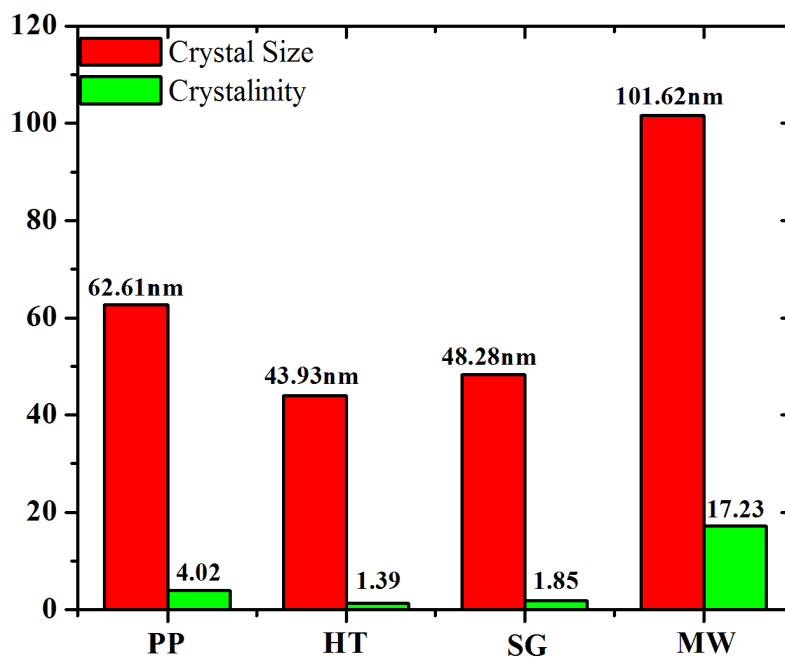


Figure.5 Comparative plot of Crystal size and crystallinity of HAp synthesized using four different methods (PP, HT, SG and MW)

Hence, crystallinity of our samples also differs with each method. E.K. Girija *et al* studied the effect sintering on thermal stability of HAp processed through precipitation method, based on the results the high temperature sintering carried out with our samples produce crystallinity [37].

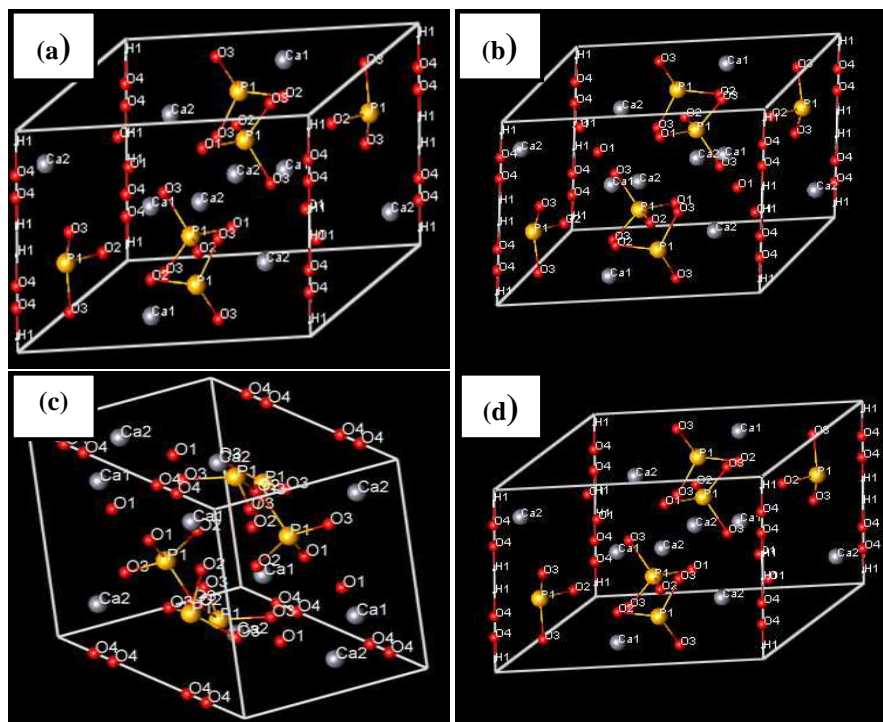


Figure.6 Crystal Structure Studies of HAp synthesized using four different methods (a) PP, (b) HT, (c) SG and (d) MW

Hydrothermal process offers direct nucleation and crystallization of HAp particles besides the high temperature aging resulted in the absence of any precursor phases like dicalcium phosphate anhydrous and dicalcium phosphate dehydrate. The higher duration of aging also enhances the above process [50,58]. A minor secondary phase of β -tricalcium phosphate was observed along with HAp in sol-gel process. The β -TCP co-precipitated as an impurity phase together with HAp, might gradually disappear as the aging time increased. Hence, a critical aging time is essential requirement for obtaining phase-pure apatite [59-60]. Moreover, HAp crystals are decomposed only after 1200°C into tricalcium phosphate and CaO. So observed TCP in our experiment is only originated as a co-precipitate during synthesis under the initial stage of reaction [61-62]. The microwave irradiation method produced better crystallinity and higher crystal size. Similar synthesis of HAp produced better resolved diffraction peaks and suggested the microwave condition promoting the mass transport to the central growing crystal from the neighboring ones resulted in growth of many more crystal planes [56].

CONCLUSION

The projected techniques for synthesis of nano Hydroxyapatite through HT, PP, SG and MW were compared for their phase purity, crystallinity, morphology and crystal size. The Influence of methodology on reaction temperature and aging condition harvested Hydroxyapatite crystals with diverse properties. Among these entrenched methods, hydrothermal method is more suitable for nano Hydroxyapatite preparation. However microwave scheme is appropriate for preparing high degree of crystalline Hydroxyapatite. The results of semi quantitative chemical analysis acquired by energy-dispersive X-ray spectroscopy (EDS) reveals superior stoichiometric HAp (Ca/P = 1.68), close to theoretical value (Ca/P = 1.67) was achieved by hydrothermal approach.

REFERENCES

- [1] MS Shojai; MT Khorasani; ED Khoshdargi; A Jamshidi. *Acta Biomater.*, **2013**, 9, 7591-7621.
- [2] K Lin; C. Wu; J Chang. *Acta Biomater.*, **2014**, 10, 4071-4102.
- [3] M Kavitha; R Subramanian; KS Vinoth; R Narayanan; G Venkatesh; N Esakkiraja. *Powder Technol.*, **2015**, 271, 167-181.
- [4] X Jin; J Zhuang; Z Zhang; H Guo; J. Tan. *J. Colloid Interface Sci.*, **2015**, 443, 125-130.

- [5] H Zhou; J Lee. *Acta Biomater.*, **2011**, 7, 2769-2781.
- [6] JS Cho; H-S Kim; S-H Um; S-H Rhee. *J. Biomed. Mater. Res., B.*, **2013**, 101B, 855-869.
- [7] B Wang; J-J Zhang; Z-Y Pana; X-Q Tao; H-S Wang. *Biosens. Bioelectron.*, **2009**, 24, 1141-1145.
- [8] L Lu; L Zhang; X Zhang; S Huan; G Shen; R Yu. *Anal. Chim. Acta.*, **2011**, 665, 146-151.
- [9] S Wang; Y. Lei; Y Zhang; J Tang; G Shen; R Yu. *Anal. Biochem.*, **2010**, 398, 191-197.
- [10] C Zhang; C Li; S Huang; Z Hou; Z Cheng; P Yang; C Peng; J Lin. *Biomaterials*, **2010**, 31, 3374-3383.
- [11] JS Son; YA Choi; EK Park; TY Kwon; KH Kim; KB Lee. *J. Biomed. Mater. Res.B.*, **2013**, 101B, 247-257.
- [12] FP Strietzel, PA Reichart, H-L Graf. *Clinical Oral Implants Research*, **2007**, 18, 743-751.
- [13] SR Bhattarai; N Bhattarai. *J Nanomed Nanotechnol.*, **2013**, 4, 3.
- [14] J Wang; LL Shaw. *Biomaterials.*, **2009**, 30, 6565-6572.
- [15] Z Fang; Q Feng. *J Mater Sci: Mater Med.*, **2014**, 35, 190-194.
- [16] RM Boehler; S Shin; AG Fast; RM Gower; LD Shea. *Biomaterials.*, **2013**, 34, 5431-5438
- [17] X Liu; Y Mou; S Wu; HC Man. *Appl. Surf. Sci.*, **2013**, 273, 748-757.
- [18] CL Tseng; KC Chang; MC Yeh; KC Yang; TP Tang; FH Lin. *Ceram. Int.*, **2014**, 40, 5117-5127.
- [19] KT Arul; JR Ramya; GM Bhalerao; SN Kalkura. *Ceram. Int.*, **2014**, 40, 13771-13779.
- [20] KP Tanul; KS Chudasama; VS Thaker; MJ Joshi. *J. Cryst. Growth.*, **2014**, 401, 474-479.
- [21] N Saha; K Keskinbora; E Suvaci; B Basu. *J. Biomed. Mater. Res., Part B*, **2010**, 95b, 2, 430-440.
- [22] Y-M Kong; S Kim; H-E Kim. *J. Am. Ceram. Soc.*, 1999, **82**, 11, 2963-68.
- [23] G Bharath; D Prabhu; D Mangalaraj; C Viswanathan; N Ponpandian. *RSC Adv.*, **2014**, 4, 50510-50520.
- [24] C Kealley; M Elcombe; AV Riessen; B-N Besim. *Physica B.*, **2006**, 385-386, 496-498.
- [25] M Kavitha; R Subramanian; R Narayanan; V Udhayabanu. *Powder Technol.*, **2014**, 253, 129-137.
- [26] V Aina; G Lusvardi; B Annaz; IR Gibson; FE Imrie; G Malavasi; L Menabue; G Cerrato; G Martra. *J. Mater. Sci. Mater. Med.*, **2012**, 23, 2335-2347,
- [27] Y Murakami; K Sugo; T Yoshitake; M Hirano; T Okuyam. *Sep. Purif. Technol.*, **2013**, 103, 161-166.
- [28] E Kramer; E Itzkowitz; M Wei. *Ceram. Int.*, **2014**, 40, 13471-13480,
- [29] S Onder; FN Kok; K Kazmanli; M Urger. *Mater. Sci. Eng., C*, **2013**, 33, 4337-4342.
- [30] Z Leilei, L Hejun, L Kezhi, F Qiangang, Z Yulei, L Shoujie. *Ceram. Int.*, **2014**, 40, 13123-13130,
- [31] O Kaygili; SV Dorozhkin; T Ates; AA Al-Ghamdi; F Yakuphanoglu. *Ceram. Int.*, **2014**, 40, 9395-9402.
- [32] S Sumathi; G Buvanewari. *Appl. Surf. Sci.*, **2014**, 303, 277-281,
- [33] Y Li; J Ho; CP Ooi. *Mater. Sci. Eng., C*, **2010**, 30, 1137-1144.
- [34] X Wang; J Zhuang; Q Peng; Y Li. *Adv Mater.*, **2006**, 18, 2031-2034.
- [35] A Bouladjine; A Al-Kattan; P Dufour; C Drouet, *Langmuir*, **2009**, 25, 12256-12265.
- [36] B Jokić; M Mitrić; V Radmilović; S Drmanić; R Petrović; D Janačković. *Ceram Int.*, **2011**, 37, 167-173.
- [37] EK Giriya; GS Kumar; A Thamizhavel; Y Yokogawa; SN Kalkura. *Powder Technol.*, **2012**, 225, 190-195.
- [38] DE Smeulders; MA Wilson; L Armstrong. *Ind.Eng. Chem.Res.*, **2001**, 40, 10.
- [39] D Yamini; GD Venkatasubbu; J Kumar; V Ramakrishnan. *Spectrochim. Acta, Part A.*, **2014**, 117, 299-303.
- [40] A Balamurugan; J Michel; J Fauré; H Benhayoune; L Wortham; G Sockalingum; V Banchet; S Bouthors; DI Maquin; G Balossier. *Ceramics – Silikáty*, **2006**, 50, 1, 27-31.
- [41] LS Taylor; G Zograf. *Pharm. Res.*, **1998**, 15, 5, 755-761.
- [42] R Sharma; RR Pandey; AA Gupta; S Kar; M Dhayal. *Mater. Chem. Phys.*, **2012**, 133, 718-725.
- [43] RG Carrodegus; SD Aza. *Acta Biomater.*, **2011**, 7, 3536-3546,
- [44] IR Gibson; W Bonfield. *J Biomed Mater Res.*, **2001**, 59, 697-708.
- [45] PN Kumta; C Sfeir; DH Lee; D Olton; D Choi. *Acta Biomater.*, **2005**, 1, 65-83,
- [46] HG Zhang; Q Zhu, *Mater Lett.*, **2005**, 59, 3054-3058.
- [47] A Rajeswari; VG Kumar; V Karthick; TS Dhas; SL Potlur. *Colloids Surf. B.*, **2013**, 111, 764-768.
- [48] LX Yang; JJ Yin; LL Wang; G-X Xing; P Yina; Q-W Liu. *Ceram Int*, **2012**, 38, 495-502.
- [49] J-G Li; T Hashida. *J. Am. Ceram. Soc.*, **2006**, 89, 3544 - 354.
- [50] MS Shojai; M-T Khorasani; A Jamshidi. *J. Cryst. Growth.*, **2012**, 361, 73-84
- [51] NK Nga; LT Giang; TQ Huy; PH Viet; C Migliaresi. *Colloids Surf. B.*, **2014**, 116, 666-673
- [52] J Klinkaewnarong; E Swatsitang; C Masingboon; S Seraphin; S Maensiri. *Curr. Appl Phys.*, **2010**, 10, 521-525.
- [53] K Lin; J Chang; Y Zhu. *Cryst. Growth Des.*, **2009**, 9, 177-181.
- [54] Y Zhang; J Lu. *J Nanopart Res*, **2007**, 9, 589-594.
- [55] U Vijayalakshmi Natarajan; S Rajeswari. *J. Cryst. Growth.*, **2008**, 310, 4601-4611.
- [56] S Meejoo; W Maneepakorn; P Winotai. *Thermochim. Acta.*, **2006**, 447, 115-120.
- [57] B-T Lee; M-H Youn; RK Paul; K-H Lee; H-Y Song. *Mater. Chem. Phys.*, **2007**, 104, 249-253.
- [58] X Zhang; KS Vecchio. *J. Cryst. Growth.*, **2007**, 308, 133-140.
- [59] F Bakan; O Laçin; H Sara. *Powder Technol.*, **2013**, 233, 295-302.
- [60] M-F Hsieh; L-H Perng; T-S Chin; H-G Perng. *Biomaterials.*, **2001**, 22, 2601-2607.
- [61] TA Kuriakose; SN Kalkura; M Palanichamy; D Arivuoli; K Dierks, G Bocelli; C. Betzel. *J. Cryst. Growth.*, **2004**, 263, 517-523.

[62]D-M Liu; T Troczynski; WJ Tseng. *Biomaterials.*, **2001**, 22, 1721-1730.